

# The von Neumann entropy for the Pearson correlation matrix: A test of the entropic brain hypothesis

H. Felipe<sup>1</sup>, A. Viol<sup>2</sup>, D. B. de Araujo<sup>3</sup>, M. G. E. da Luz<sup>4</sup>, F.

Palhano-Fontes<sup>3</sup>, H. Onias<sup>3</sup>, E. P. Raposo<sup>5</sup>, G. M. Viswanathan<sup>1,6</sup>

<sup>1</sup>*Department of Physics, Federal University of Rio Grande do Norte, Natal-RN, 59078-970, Brazil*

<sup>2</sup>*Cognitive Neuroscience, Scuola Internazionale Superiore di Studi Avanzati, Trieste, 34136, Italy*

<sup>3</sup>*Brain Institute, Federal University of Rio Grande do Norte, Natal-RN, 59078-970, Brazil*

<sup>4</sup>*Departamento de Física, Universidade Federal do Paraná, Curitiba-PR, 81531-980, Brazil*

<sup>5</sup>*Laboratório de Física Teórica e Computacional, Departamento de Física, Universidade Federal de Pernambuco, Recife-PE, 50670-901, Brazil*

<sup>6</sup>*National Institute of Science and Technology of Complex Systems, Federal University of Rio Grande do Norte, Natal-RN, 59078-970, Brazil*

(Dated: June 11, 2021)

We address the general problem of how to estimate an entropy given a Pearson correlation matrix. Most methods currently in use inject a degree of arbitrariness due to the thresholding of correlations. Here we propose an entirely objective method of entropy estimation that requires no thresholding. Let  $\mathbf{R}$  be an  $N \times N$  Pearson correlation matrix. We define the matrix  $\boldsymbol{\rho} = \mathbf{R}/N$  and prove that  $\boldsymbol{\rho}$  satisfies all the properties required of the density operator. Hence, the von Neumann entropy  $S = -\text{tr}(\boldsymbol{\rho} \log \boldsymbol{\rho})$  can be directly calculated from the Pearson correlation matrix. To demonstrate the generality and power of the method, we estimate the entropy of functional correlations of the human brain. We find that the entropy increases for altered brain states under serotonergic agonist action, as predicted by the entropic brain hypothesis.

An important open problem in physics concerns how to estimate the entropy from the Pearson correlation matrix of an arbitrary data set [1–3]. This problem has wide and immediate applicability to diverse phenomena, e.g., correlated asset prices [4, 5], diffusion processes [6, 7], and brain networks [8–10]. The Shannon entropy solves the simpler problem of how to calculate the entropy given a probability distribution [11]. However, attempts to extend this formalism to estimate the entropy of a correlation matrix have required admittedly *ad hoc* methods, such as the thresholding of the correlation matrix to generate a new symmetric and unweighted adjacency matrix consisting only of 0's and 1's [12, 13]. The resulting adjacency matrix represents a simple graph, which can then be studied using topological metrics. These methods have led to significant advances in diverse fields, examples of which include applications to market volatility in financial crisis [14], and to scale-free and small-world brain networks [15, 16]. Nevertheless, they have drawbacks that motivate the search for better approaches [17].

The main limitation of the existing methods is that the thresholding operation inevitably leads to loss of information [18]. Consider, for example, the set of all possible  $2 \times 2$  Pearson correlation matrices. Since a correlation coefficient can assume any real value in the closed interval  $[-1, 1]$ , there are an infinite number of possible  $2 \times 2$  Pearson matrices. In contrast, there are only two corresponding adjacency matrices of size  $2 \times 2$  because a simple graph with 2 nodes is either connected or disconnected. Significant information can thus be lost due to thresholding. Moreover, the results are not always adequately robust with respect to the choice of

thresholding [19, 20]. Insofar as unweighted matrices are used, these methods are only indirectly measuring the entropy of correlations, generally via topological metrics such as network motifs [21], degree distribution [22], and geodesic diversity [23]. There is thus a growing and vexing demand for a better method of estimating entropy.

Here, we show that the problem of how to calculate the entropy of a correlation matrix is akin to one solved long ago by John von Neumann [24] and Lev Landau [25] for the density operator

$$\boldsymbol{\rho} = \sum_{i=1}^M p_i |\psi_i\rangle\langle\psi_i| \quad (1)$$

that describes an ensemble of  $M$  state vectors  $|\psi_i\rangle$  with assigned classical probabilities  $p_i$  [26]. Given a density operator  $\boldsymbol{\rho}$  with  $N$  eigenvalues  $\lambda_j$ , the von Neumann entropy is defined according to

$$S(\boldsymbol{\rho}) = -\text{tr}(\boldsymbol{\rho} \log \boldsymbol{\rho}) = -\sum_{j=1}^N \lambda_j \log \lambda_j. \quad (2)$$

It is well known that a linear operator  $\boldsymbol{\rho}$  must satisfy three necessary and sufficient conditions for the von Neumann entropy to be well defined:  $\boldsymbol{\rho}$  must (i) be Hermitian, (ii) have unit trace, and (iii) be positive semidefinite (i.e., the eigenvalues must be non-negative). Given an arbitrary Pearson correlation matrix, we will show below how to construct a corresponding density matrix. This procedure will thereby allow the calculation of the von Neumann entropy from the Pearson matrix.

We first review the definition of the Pearson correlation matrix. Consider  $N$  data sets, each with a population

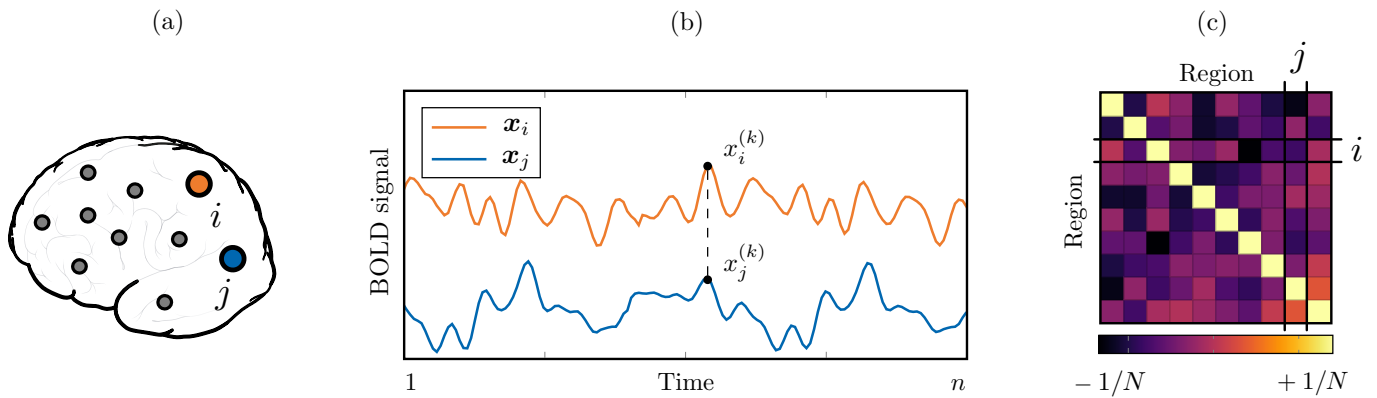


Figure 1. The construction of a density matrix from a Pearson correlation matrix. (a) The system of interest (say, the brain) is partitioned into  $N$  interacting components or nodes (regions). The  $i$ -th and  $j$ -th regions are shown highlighted. (b) The correlation between regions  $i$  and  $j$  is then calculated. For each  $i$  region there are  $n$  data points  $x_i^{(k)}$  where  $k = 1, \dots, n$ . In the example of the brain that we study here, the  $x_i^{(k)}$  represent fluctuations of the blood-oxygen-level-dependent (BOLD) signal for region  $i$ . The correlation  $R_{ij}$  between regions  $i$  and  $j$  is given by Eq. (3), and lies in the interval  $-1 \leq R_{ij} \leq 1$ . (c) For each correlation coefficient  $R_{ij}$ , we calculate  $\rho_{ij} = R_{ij}/N$ , yielding the matrix  $\rho = \mathbf{R}/N$ . This matrix  $\rho$  fully satisfies the properties of a density operator, i.e., (i) hermiticity, (ii) unit trace, and (iii) positive semidefiniteness. Finally, we calculate the von Neumann entropy from this density matrix, via (2). Panel (a) is adapted from [32].

of  $n$  measurements. Let  $\mathbf{x}_i = (x_i^{(1)}, \dots, x_i^{(n)})$  denote the sequence of  $n$  measurements of the  $i$ -th data set. Let  $\langle \cdot \rangle$  denote the average taken over the population of  $n$  points, so that  $\mathbf{X}_i = \mathbf{x}_i - \langle \mathbf{x}_i \rangle$  represents deviations from the mean  $\langle \mathbf{x}_i \rangle$  and  $\sigma_i^2 = \langle \mathbf{X}_i^2 \rangle$  is the variance of  $\mathbf{x}_i$ . The correlation between the  $i$ -th and  $j$ -th data sets is then given by the Pearson correlation coefficient

$$R_{ij} = \frac{1}{n} \sum_{k=1}^n \left[ \frac{x_i^{(k)} - \langle \mathbf{x}_i \rangle}{\sigma_i} \right] \left[ \frac{x_j^{(k)} - \langle \mathbf{x}_j \rangle}{\sigma_j} \right] = \frac{\langle \mathbf{X}_i \mathbf{X}_j \rangle}{\sigma_i \sigma_j}. \quad (3)$$

The Pearson correlation matrix is the  $N \times N$  matrix  $\mathbf{R}$  with entries  $R_{ij}$  given by (3).

Given a Pearson correlation matrix  $\mathbf{R}$ , the entropy is often estimated by using a different (but related) object as a proxy, viz., a binary adjacency matrix  $\mathbf{A}$ . The latter is defined by imposing a threshold value  $\xi$  over the entries of  $\mathbf{R}$ . Specifically, one sets  $A_{ij} = 1$  whenever  $|R_{ij}| \geq \xi$  for  $i \neq j$ , and  $A_{ij} = 0$  otherwise [27]. The matrix  $\mathbf{A}$  defines a graph with  $N$  nodes and undirected and unweighted edges. The entropy estimation, then, becomes a matter of computing the Shannon entropy of certain probability distributions embedded in the graph structure of  $\mathbf{A}$ , as explained earlier. We note that, in network analysis, the von Neumann entropy has previously been used with adjacency matrices [28, 29], however it has never been applied directly to Pearson correlation matrices.

Numerous properties of correlation matrices can be extracted from their thresholded counterparts, partly due to the information that remains stored in the topology of simple graphs [30]. Hence, these methods have become pivotal and ubiquitous in the study of complex systems [14–16]. But there are yet other drawbacks to

this approach, in addition to the limitations previously mentioned [17–20]. Not only can thresholding lead to loss of information, it can even inject spurious complexity into genuinely random networks [31]. For these reasons, such methods require caution when applied to real-world networks [10].

In order to overcome these difficulties, we develop a way to estimate the entropy directly from the Pearson correlation matrix, without the intermediary step requiring an adjacency matrix. Our method rests on the following mathematical foundation: if  $\mathbf{R}$  is an arbitrary  $N \times N$  Pearson correlation matrix, then

$$\rho = \frac{\mathbf{R}}{N} \quad (4)$$

satisfies all the conditions for a density operator: (i) hermiticity, (ii) unit trace, and (iii) positive semidefiniteness. To see this, observe that  $\mathbf{R}$  has real and symmetric entries, from which follows claim (i). Next, the diagonal entries are given by

$$R_{ii} = \frac{\langle \mathbf{X}_i^2 \rangle}{\sigma_i^2} = 1, \quad (5)$$

so that  $\text{tr} \mathbf{R} = N$ , leading to claim (ii). For (iii), it suffices to show that  $\mathbf{R}$  is positive semidefinite. In other words, we must show that  $\mathbf{v} \cdot \mathbf{R} \mathbf{v} \geq 0$  for all  $\mathbf{v} \in \mathbb{R}^N$ . In fact, the positive semidefiniteness of Pearson correlation matrices is well known. Observe that

$$\sum_{ij} v_i \left( \sum_k X_i^{(k)} X_j^{(k)} \right) v_j = \sum_k \left| \sum_i v_i X_i^{(k)} \right|^2 \geq 0. \quad (6)$$

We now state our main result. Given an arbitrary Pearson correlation matrix, the entropy can be calculated

from Eq. (2), with  $\rho$  given by (4). We illustrate our general method in Figure 1. We remark in passing that many other correlation matrices (e.g., Spearman, Kendall) will satisfy analogous conditions, so long as they consist of real symmetric entries [33].

Next we give illustrative examples of maximal and minimal entropies for  $N$  data sets. Consider first the scenario where all  $\mathbf{x}_i$  and  $\mathbf{x}_j$  are statistically independent, i.e., uncorrelated:  $\langle \mathbf{X}_i \mathbf{X}_j \rangle = \langle \mathbf{X}_i^2 \rangle \delta_{ij}$ . Thus  $R_{ij} = \delta_{ij}$ , and, as expected, the density operator admits the (completely mixed state) representation  $\rho = \mathbf{I}/N$ , where  $\mathbf{I}$  is the  $N \times N$  identity matrix. The von Neumann entropy then assumes the maximal value of  $S = \log N$ , as it should.

Compare the above with the other extreme, i.e., when all pairs are perfectly autocorrelated, so that  $\mathbf{X}_i/\sigma_i = \mathbf{X}_j/\sigma_j$  for all  $i, j$ . Then, clearly,  $R_{ij} = 1$ , so that  $\mathbf{R}^2 = N\mathbf{R}$ . The density operator is thus idempotent:  $\rho^2 = \rho$ . It follows immediately that

$$\text{tr}(\rho \log \rho) = \text{tr}(\rho \log \rho^2) = 2 \text{tr}(\rho \log \rho),$$

hence  $\text{tr}(\rho \log \rho) = 0$ . Therefore, the von Neumann entropy assumes  $S = 0$ , which is the absolute minimum possible value (corresponding to a pure state configuration).

We thus have a robust and direct approach to obtain the entropy of correlation matrices. Crucially, at no point have we introduced *a priori* estimates, hence the resulting entropy is free from arbitrary or extraneous assumptions (e.g., choice of threshold  $\xi$ ). Of course, one can additionally use thresholding to obtain a suitable  $\mathbf{A}$ , but even then our protocol can still be useful. For example, it can be used to obtain an exact expression for the entropy of an idealized ranked set of correlated data (see Supplemental Material [34]). Such results might then yield a null hypothesis for subsequent statistical inference or to undertake more rigorous hypothesis testing.

As a practical demonstration of the method's power and wide applicability, we calculate the entropy of Pearson correlation matrices obtained from functional magnetic resonance imaging (fMRI) of the human brain [44]. Specifically, we test the hypothesis of increased brain entropy while under the influence of a psychedelic [45]. For this purpose, we chose the indigenous beverage ayahuasca [46], a decoction with rapid antidepressant effects partially mediated by the serotonergic agonist *N,N*-dimethyltryptamine (DMT) [47–49].

A total of 9 healthy human volunteers were assigned to a neuroimaging session both before and after ayahuasca intake. We have a set of  $N = 104$  fMRI time series of the BOLD signal of the human brain from each subject at both conditions. See, again, the Supplemental Material [34] for details on the method of parcellating the brain into regions of interest, of acquiring the fMRI images, and of obtaining the BOLD time series.

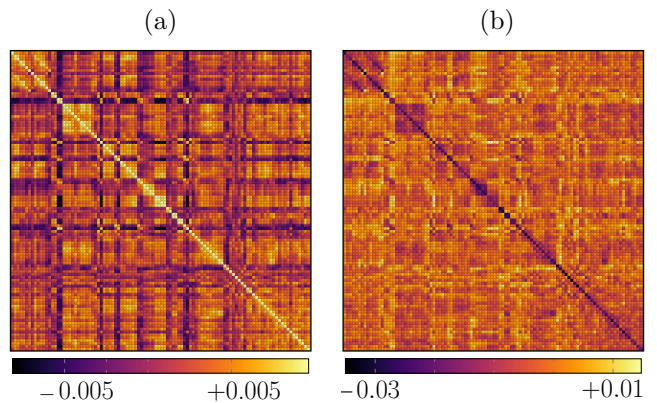


Figure 2. Functional connectivity of the brain of a volunteer (Subject 4) in the ayahuasca condition. (a) Matrix with entries  $\rho_{ij} = R_{ij}/N$ , where  $R_{ij}$  is the Pearson correlation of the  $i$ -th and  $j$ -th BOLD fMRI time series. (b) The matrix  $\rho \log \rho$ . Up to a sign, the trace of  $\rho \log \rho$  gives the von Neumann entropy of  $\rho$ .

We next calculated the density operators. The 18 correlation matrices were individually scaled according to Eq. (4) using  $N = 104$ . Figure 2(a) shows an example of the functional connectivity network (represented as a matrix) from a single subject in the ayahuasca condition. Every matrix entry  $\rho_{ij}$  is shown ( $i, j = 1, \dots, 104$ ), expressing the (scaled) correlation between pairs of time series  $\mathbf{x}_i$  and  $\mathbf{x}_j$ . In 2(b), the matrix  $\rho \log \rho$  is also shown in its entirety. Up to a sign, the sum of its diagonal entries is precisely the von Neumann entropy of  $\rho$ .

Figure 3 shows the normalized entropy of all 18 matrices  $\rho$ , grouped in terms of subjects (from 1 to 9) for both experimental conditions (before and after ayahuasca ingestion). With the exception of 2 individuals (Subjects 1 and 9), we find positive entropy variation  $\Delta S \equiv S_{\text{after}} - S_{\text{before}}$  among subjects (dotted lines). However, the low number of individuals demands careful analysis in regards to statistical significance.

The relevance of our method's findings is best seen through the lens of the entropic brain hypothesis (EBH) [45], a recent approach to cognitive neuroscience grounded on notions of criticality [55, 56] and prompted by neuroimaging research with psychedelic compounds (e.g., psilocybin, LSD) [51, 57, 58]. The EBH asserts that the quality of conscious states is dependent upon the entropy of key parameters of brain function. Specifically, it predicts an increase of entropy when the brain is under the influence of a psychedelic substance.

Through various indirect measures of spontaneous brain activity, the EBH was shown consistent with previously conducted works, for instance, the enhanced repertoire of network motifs post-psilocybin infusion [21], the greater sample entropy (negative predictability) of fMRI time courses following LSD administration [59], as

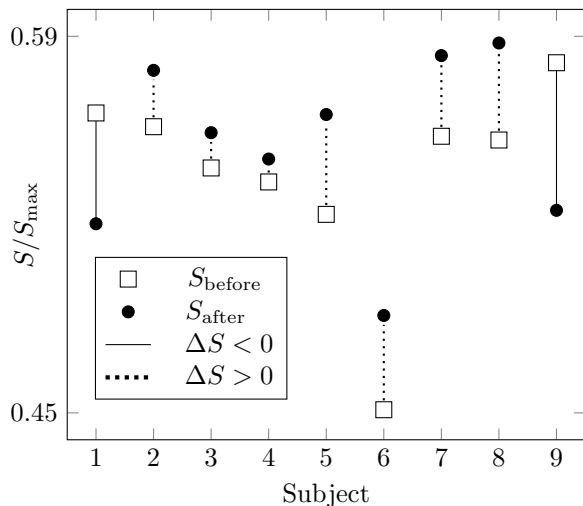


Figure 3. Entropy before and after ayahuasca. The plot shows the von Neumann entropy  $S$  of the 9 subjects (horizontal axis), both before ( $S_{\text{before}}$ ) and after ( $S_{\text{after}}$ ) ayahuasca ingestion, normalized by  $S_{\text{max}} = \log(104)$ . Entropy variation  $\Delta S = S_{\text{after}} - S_{\text{before}}$  was found positive for 7 subjects (dotted lines). These findings are broadly consistent with the entropic brain hypothesis, although one must be careful due to the small number of subjects involved.

well as with the broadening of functional patterns due to ayahuasca intake [22, 23]. In this work, similarly, we found increases in brain entropy among individuals in the ayahuasca condition. Specifically, the entropy of correlations embedded in the functional connectivity of the human cortex (i.e., correlated BOLD fMRI time series) increases in 7 out of 9 subjects undergoing the effects of ayahuasca. Our test of the entropic brain hypothesis requires careful interpretation because of the small sample size. Indeed, the main goal of this work is to show the generality and usefulness of the proposed method based on the von Neumann entropy, as a proof of concept. It should be clear to the reader that the proposed method can be used to perform rigorous hypothesis testing on arbitrarily large data sets, for example.

From a methodological standpoint, it is instructive to compare our results with those of Viol *et al.* in [22] and [23]: following the ayahuasca consumption, the latter found an enhanced neighborhood diversity (as measured by the geodesic entropy) of the nodes within functional networks; whereas the former measured a greater entropy of the network’s degree distribution. Crucially, both works applied a range of threshold values to examine the properties of numerous adjacency matrices. This was done in an effort to compensate for the inherent limitations of the thresholding procedure. In contrast, the method here proposed uses no thresholding in its entropy calculation, thus evading the drawbacks associated with thresholding [17–20, 31]. Calculation

of the von Neumann entropy is also fast, for it uses a single correlation matrix instead of many adjacency matrices. Moreover, the von Neumann entropy has a solid mathematical foundation [26].

The concept of entropy has found growing importance within the general area of biomedicine, particularly in neuroscience. Indeed, entropic features of the brain activity have recently served as the basis for new models of brain function and structure [60–62]. On such grounds, the present protocol should be considered a relevant new addition to the existing tools to analyze functional correlations in the human brain. For instance, it has corroborated the view that psychedelics induce brain entropy increase. Finally, in a broader context we believe our approach can be successfully applied to many other complex systems, such as risk management in financial markets [63], and the dynamics of disease spreading and information routing [64, 65].

We thank M. Copelli and S. Ribeiro for discussions. AV thanks the support of PRIN grant 20174TPEFJ “TRIPS”. This work was supported by the Brazilian agencies CNPq (Grants No. 304532/2019-3, No. 305062/2017-4 and No. 302051/2018-0), CAPES, and FACEPE.

- 
- [1] R. Albert and A. Barabási, *Rev. Mod. Phys.* **74**, 47 (2002).
  - [2] K. Anand and G. Bianconi, *Phys. Rev. E* **80**, 045102(R) (2009).
  - [3] M. De Domenico and J. Biamonte, *Phys. Rev. X* **6**, 041062 (2016).
  - [4] A. Almog and E. Shmueli, *Sci. Rep.* **9** 10832 (2019).
  - [5] A. Chakraborti, Hrishidev, K. Sharma, and H. K. Pharasi, *J. Phys. Complex.* **2**, 015002 (2021).
  - [6] J. Gómez-Gardeñes and V. Latora, *Phys. Rev. E* **78**, 065102(R) (2008).
  - [7] P. Holme and J. Saramäki, *Phys. Rep.* **519**, 97 (2012).
  - [8] E. Bullmore and O. Sporns, *Nat. Rev. Neurosci.* **10**, 186 (2009).
  - [9] F. A. N. Santos, E. P. Raposo, M. D. Coutinho-Filho, M. Copelli, C. J. Stam, and L. Douw, *Physical Review E* **100**, 032414 (2019)
  - [10] C. Nicolini, G. Forcellini, L. Minati, and A. Bifone, *Neuroimage* **211**, 116603 (2020).
  - [11] C. Shannon, *Bell System Tech. J.* **27** 623 (1948).
  - [12] V. Latora and M. Marchiori, *Phys. Rev. Lett.* **87**, 198701 (2001).
  - [13] X. Yan, L. G. S. Jeub, A. Flammini, F. Radicchi, and S. Fortunato, *Phys. Rev. E* **98**, 042304 (2018).
  - [14] S. Kumar and N. Deo, *Phys. Rev. E* **86**, 026101 (2012).
  - [15] V. M. Eguíluz, D. R. Chialvo, G. A. Cecchi, M. Baliki, and A. V. Apkarian, *Phys. Rev. Lett.* **94**, 018102 (2005).
  - [16] D. S. Bassett and E. Bullmore, *The Neuroscientist* **12**, 512 (2006).
  - [17] M. Rubinov and O. Sporns, *Neuroimage* **56**, 2068 (2011).
  - [18] V. Kukreti, H. K. Pharasi, P. Gupta, and S. Kumar, *Front. Phys.* **8**, 323 (2020).

- [19] N. Langer, A. Pedroni, and L. Jäncke, *PLOS ONE* **8**, 1 (2013).
- [20] K. A. Garrisona, D. Scheinostb, E. S. Finn, X. Shenb, R. T. Constablebd, *Neuroimage* **118**, 651 (2015).
- [21] E. Tagliazucchi, R. L. Carhart-Harris, R. Leech, D. Nutt, and D. R. Chialvo, *Hum. Brain Mapp.* **35**, 5442 (2014).
- [22] A. Viol, F. Palhano-Fontes, H. Onias, D. B. de Araujo, and G. M. Viswanathan, *Sci. Rep.* **7**, 7388 (2017).
- [23] A. Viol, F. Palhano-Fontes, H. Onias, D. B. de Araujo, P. Hövel, and G. M. Viswanathan, *Entropy* **21**, 128 (2019).
- [24] J. von Neumann, *Thermodynamik quantenmechanischer Gesamtheiten*, Nachr. Ges. Wiss. Göttingen (1927).
- [25] L. D. Landau, The Damping Problem in Wave Mechanics, in *Collected Papers of L.D. Landau*, edited by D. T. Haar (Pergamon, 1965), pp. 8-18.
- [26] M. Ohya and D. Petz, *Quantum Entropy and Its Use* (Springer-Verlag, Berlin, 1993).
- [27] Y. Liu, M. Liang, Y. Zhou, Y. He, Y. Hao, M. Song, C. Yu, H. Liu, Z. Liu, and T. Jiang, *Brain* **131**, 945 (2008).
- [28] F. Passerini and S. Severini, *Int. J. Agent Tech. Syst.* **1** 58 (2009).
- [29] E. Estrada, J. A. de la Peña, and N. Hatano, *Linear Algebra Appl.* **443**, 235 (2014).
- [30] A. Viol, V. Vuksanović, and P. Hövel, *Physica A* **561**, 125233 (2021).
- [31] G. T. Cantwell, Y. Liu, B. F. Maier, A. C. Schwarze, C. A. Serván, J. Snyder, and G. St-Onge, *Phys. Rev. E* **101**, 062302 (2020).
- [32] P. J. Lynch and C. C. Jaffe, *CC BY 2.5* (2006).
- [33] K. Boudt, J. Cornelissen, and C. Croux, *Stat. Comput.* **22**, 471 (2012).
- [34] See Supplemental Material at PRL-link for a detailed description of the experimental procedure, data acquisition, and mathematical analysis. It includes Refs. [35–43] and [50–54].
- [35] L. Guttman, The quantification of a class of attributes: a theory and method of scale construction, in *The prediction of personal adjustment*, edited by P. Horst, P. Wallin, L. Guttman, F. B. Wallin, J. A. Clausen, R. Reed, and E. Rosenthal (Social Science Research Council, New York, 1941), pp. 319-348.
- [36] L. Guttman, The principal components of scale analysis, in *Measurement and prediction*, edited by S. A. Stouffer, L. Guttman, E. A. Suchman, P. F. Lazarsfeld, S. A. Star, and J. A. Clausen (Princeton University Press, Princeton, 1950), pp. 312-361.
- [37] R. Zwick, *Psychometrika* **52**, 512 (1987).
- [38] C. P. Davis-Stober, J.-P. Doignon, and R. Suck, *Front. Psychol.* **6**, 1767 (2015).
- [39] M. Kendall, *Rank Correlation Methods*, 5th ed. (Oxford University Press, Oxford, 1990).
- [40] L. Piao and Z. Fu, *Sci. Rep.* **6**, 36759 (2016).
- [41] L. A. Goodman, *J. Am. Stat. Assoc.* **70**, 755 (1975).
- [42] D. J. Hand, *J. R. Statist. Soc. A* **159**, 445 (1996).
- [43] C. H. Coombs, L. C. Coombs, and J. C. Lingoos, Stochastic cumulative scales, *Theory construction and data analysis in the behavioral sciences*, edited by S. Shye (Jossey-Bass, San Francisco, 1978), pp. 280–298.
- [44] S. M. Smith, *Neuroimage* **62**, 1257 (2012).
- [45] R. L. Carhart-Harris, R. Leech, P. J. Hellyer, M. Shanahan, A. Feilding, E. Tagliazucchi, D. R. Chialvo, and D. Nutt, *Front. Hum. Neurosci.* **8**, 20 (2014).
- [46] L. E. Luna, Indigenous and Mestizo use of Ayahuasca. An Overview, in *The Ethnopharmacology of Ayahuasca*, edited by R. G. dos Santos (Transworld Research Network, Tivandrum, 2011), pp 1-21.
- [47] J. Riba, M. Valle, G. Urbano, M. Yritia, A. Morte, and M. J. Barbanøj, *J. Pharmacol. Exp. Ther.* **306**, 73 (2003).
- [48] F. L. Osório, R. F. Sanches, L. R. Macedo, R. G. dos Santos, J. P. Maia-de-Oliveira, L. Wichert-Ana, D. B. de Araujo, J. Riba, J. A. Crippa, and J. E. Hallak, *Rev. Bras. Psiquiatr.* **37**, 13 (2015).
- [49] F. Palhano-Fontes, D. Barreto, H. Onias, K. C. Andrade, M. M. Novaes, J. A. Pessoa, S. A. Mota-Rolim, F. L. Osório, R. Sanches, R. G. dos Santos *et al.*, *Psychol. Med.* **49**, 655 (2019).
- [50] A. P. Association, Diagnostic and Statistical Manual of Mental Disorders: DSM-IV-TR (American Psychiatric Association, 2000).
- [51] D. B. de Araujo, S. Ribeiro, G. A. Cecchi, F. M. Carvalho, T. A. Sanchez, J. P. Pinto, B. S. de Martinis, J. A. Crippa, J. E. C. Hallak, and A. C. Santos, *Hum. Brain Mapp.* **33**, 255 (2012).
- [52] M. Jenkinson, C. F. Beckmann, T. E. Behrens, M. W. Woolrich, and S. M. Smith, *Neuroimage* **62** 782 (2012).
- [53] M. Brett, I. S. Johnsrude, and A. M. Owen, *Nat. Rev. Neurosci.* **3**, 243 (2002).
- [54] H. Onias, A. Viol, F. Palhano-Fontes, K. C. Andrade, M. Sturzbecher, G. Viswanathan, and D. B. de Araujo, *Epilepsy Behav.* **38**, 71 (2014).
- [55] O. Kinouchi and M. Copelli, *Nat. Phys.* **2**, 348 (2006).
- [56] D. R. Chialvo, *Nat. Phys.* **6**, 744 (2010).
- [57] R. L. Carhart-Harris, D. Erritzoe, T. Williams, J. M. Stone, L. J. Reed, A. Colasanti, R. J. Tyacke, R. Leech, A. L. Malizia, K. Murphy *et al.*, *PNAS* **109**, 2138 (2012).
- [58] R. L. Carhart-Harris, S. Muthukumaraswamy, L. Roseman, M. Kaelen, W. Droog, K. Murphy, E. Tagliazucchi, E. E. Schenberg, T. Nest, C. Orban *et al.*, *PNAS* **113**, 4853 (2016).
- [59] A. V. Lebedev, M. Kaelen, M. Lövdén, J. Nilsson, A. Feilding, D. J. Nutt, and R. L. Carhart-Harris, *Hum. Brain Mapp.* **37**, 3203 (2016).
- [60] R. L. Carhart-Harris and K. J. Friston, *Neuropharmacology* **71**, 316 (2019).
- [61] R. Herzog, P. A. M. Mediano, F. E. Rosas, R. Carhart-Harris, Y. S. Perl, E. Tagliazucchi, and R. Cofre, *Sci. Rep.* **10**, 17725 (2020).
- [62] C. Sanz, C. Pallavicini, F. Carrillo, F. Zamberlan, M. Sigman, N. Mota, M. Copelli, S. Ribeiro, D. Nutt, R. Carhart-Harris, and E. Tagliazucchi, *Conscious. Cogn.* **87**, 103070 (2021).
- [63] A. Namaki, A. Shirazi, R. Raei, and G. Jafari, *Physica A* **390**, 3835 (2011).
- [64] S. Boccaletti, V. Latora, Y. Moreno, M. Chavez, and D. -U. Hwang, *Phys. Rep.* **424**, 175 (2006).
- [65] I. Iacopini, S. Milojević, and V. Latora, *Phys. Rev. Lett.* **120**, 048301 (2018).

**Supplementary Material for:**  
**The von Neumann entropy for the Pearson correlation matrix:**  
**A test of the entropic brain hypothesis**

H. Felipe<sup>1</sup>, A. Viol<sup>2</sup>, D. B. de Araujo<sup>3</sup>, M. G. E. da Luz<sup>4</sup>, F. Palhano-Fontes<sup>3</sup>, H. Onias<sup>3</sup>, E. P. Raposo<sup>5</sup>, G. M. Viswanathan<sup>1,6</sup>

<sup>1</sup>*Department of Physics, Federal University of Rio Grande do Norte, Natal–RN, 59078-970, Brazil*

<sup>2</sup>*Cognitive Neuroscience, Scuola Internazionale Superiore di Studi Avanzati, Trieste, 34136, Italy*

<sup>3</sup>*Brain Institute, Federal University of Rio Grande do Norte, Natal–RN, 59078-970, Brazil*

<sup>4</sup>*Departamento de Física, Universidade Federal do Paraná, Curitiba-PR, 81531-980, Brazil*

<sup>5</sup>*Laboratório de Física Teórica e Computacional, Departamento de Física, Universidade Federal de Pernambuco, Recife-PE, 50670-901, Brazil*

<sup>6</sup>*National Institute of Science and Technology of Complex Systems, Federal University of Rio Grande do Norte, Natal–RN, 59078-970, Brazil*

(Dated: June 11, 2021)

## I. GUTTMAN SCALING

### A. The von Neumann entropy for the Homogeneous Guttman-scalable Pearson correlation matrix

Here we discuss an idealized type of data, following the Guttman scaling [35, 36]. In the homogeneous case [37] (see below), many exact results are known for the corresponding Pearson correlation matrix  $\mathbf{R}_{hG}$  [37, 38]. As we will show, this allows to write an analytical expression for the von Neumann entropy  $S_{hG}$  of  $\mathbf{R}_{hG}$ . Although real data rarely fits in with a perfect Guttman scale, the present  $S_{hG}$  could play the role of a null hypothesis model [37]. Indeed, it may be useful for testing hierarchies as well as features of correlations in distinct processes involving  $N$  populations [39, 40]; in our case all with the same size  $n$  and described by ( $i = 1, \dots, N$ )

$$\mathbf{x}_i = (x_i^{(1)}, \dots, x_i^{(n)}) . \quad (\text{S1})$$

Moreover, Guttman scaling is a very instructive example of how the von Neumann entropy portrays data with strong but not absolute correlations.

Next we address (homogeneous) Guttman-scalable data as usually done in the literature [37, 41]. Possible ways to relate such standard framework to data in the form of Eq. (S1) is briefly considered in Sec. IB. For our purposes, we concentrate on dichotomous or binary events (or “items”, a more common terminology in the area of statistical measurement theory [37, 42]). Thus, to each properly defined event  $i$  we can associate two distinct numerical values, 0 and 1. For a given instance or realization pattern for the collection of events, the numerical value 1 (0) for the event  $i$  means it has (has not) taken place in that pattern.

The idea underlying the Guttman scaling, also known as cumulative scaling or scalogram analysis, is to be able to create a table or indicator matrix — which should

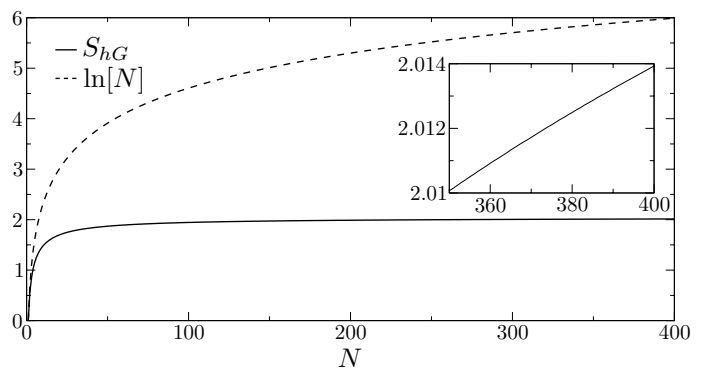


Figure S1. The von Neumann entropy,  $S_{hG}$ , for a Pearson correlation matrix resulting from an ideal homogeneous Guttman-scalable data set versus its population (or items) number  $N$ . The entropy  $S_{hG}$  tends to a constant value for  $N$  going to infinity (see the inset). For comparison, it also shows the von Neumann entropy for a completely uncorrelated data set, for which  $S = \ln[N]$ .

not be confused with the correlation matrix  $\mathbf{R}$  itself — assembling the data in a very particular manner. If such construction is possible for the data set, the indicator matrix would display a triangular structure, with all entries in the lower (upper) part equal to 1 (0), see Table I. Hence, within a given pattern of outcomes, there is a priority of events. If the event  $i$  has occurred, then event  $i - 1$  has also occurred. The Table I explains in more detail the data organization.

Two extra assumptions for data already observing the Guttman arrangement are known as homogeneity conditions [37]. They can be stated as the following. (a) There is no full correlation between any two populations  $\mathbf{x}_{i'}$  and  $\mathbf{x}_{i''}$ . Actually, in many contexts this is not a really restrictive hypothesis, either because such coincidence is rare or, if it is not, for  $N$  large enough we can just eliminate the akin  $\mathbf{x}_i$ 's from the data set without losing relevant statistical significance. (b)

Table I. The data table (or indicator matrix) organized in a specific ordering of events  $i$ , with  $i = 1, \dots, N$ . Along each row — representing a particular configuration of events occurrence: a pattern — the entry 1 (0) means that the corresponding event has (has not) taken place. The depicted structure illustrates a perfect Guttman scaling: for the pattern  $i$ , only the events up to  $i - 1$  do take place. This ascribes a ranking or degree of prevalence among the distinct events within a specific pattern.  $\mathcal{N}_i$  is the number of times the pattern  $i$  is found in the full data set collection.

Pattern	Event 1	Event 2	Event 3	Event 4	Event 5	...	Event $N$	Number of occurrences
1	0	0	0	0	0	...	0	$\mathcal{N}_1$
2	1	0	0	0	0	...	0	$\mathcal{N}_2$
3	1	1	0	0	0	...	0	$\mathcal{N}_3$
4	1	1	1	0	0	...	0	$\mathcal{N}_4$
5	1	1	1	1	0	...	0	$\mathcal{N}_5$
6	1	1	1	1	1	...	0	$\mathcal{N}_6$
$\vdots$	$\vdots$	$\vdots$	$\vdots$	$\vdots$	$\vdots$	$\vdots$	0	$\vdots$
$N + 1$	1	1	1	1	1	...	1	$\mathcal{N}_{N+1}$

The probability of obtaining the different patterns of outcomes indicated in Table I (see also Sec. IB) are the same, i.e., the  $\mathcal{N}_i$ 's in Table I are essentially all equal. Arguably, this may seem a too restricting imposition [38]. But perhaps a bit surprising, it has been verified numerically that certain results (like principal component analysis and certain properties of covariance matrices) for homogeneous data do not depart very much from the case where the  $\mathcal{N}_i$ 's display a normal distribution (provided the populations have ample variability [37, 38]).

Therefore, it is correct to affirm that data obeying the homogeneous Guttman scaling is not ubiquitous. But the relevant fact for our purposes is that, precisely because of that, the Pearson correlation matrix  $\mathbf{R}_{hG}$  can be derived analytically [37]. Furthermore, its exact eigenvalues  $\tilde{\lambda}_i$ 's have been obtained in [37]. Since the eigenvalues  $\lambda_i$ 's of  $\rho_{hG}$  are simply  $\tilde{\lambda}_i/N$ , then from [37] we get

$$\lambda_i = \frac{1 + N^{-1}}{i(i+1)}. \quad (\text{S2})$$

Notice that the  $\lambda_i$ 's depend only on a single parameter, the population number  $N$ . So, finally we find

$$\begin{aligned} S_{hG} &= -(1 + N^{-1}) \sum_{i=1}^N \frac{1}{i(i+1)} \ln \left[ \frac{1 + N^{-1}}{i(i+1)} \right] \\ &= \ln[N] - (1 - N^{-2}) \ln[N + 1] \\ &\quad + 2(1 + N^{-1}) \sum_{i=1}^{N-1} \frac{1}{i(i+2)} \ln[i + 1]. \end{aligned} \quad (\text{S3})$$

Since it is well known that the series  $\sum_{i=1}^{\infty} \ln[i]/i^2$  converges, it is not difficult to prove that  $S_{hG}$  also converges as  $N \rightarrow \infty$ . Also, due to the peculiar way items are correlated in a homogeneous Guttman-scalable data collection, after a rapid increase with  $N$ , the entropy  $S_{hG}$  tends to a plateau as  $N$  increases. Figure S1 illustrates the general behavior of  $S_{hG}(N)$ , also comparing it with the von Neumann entropy for a Pearson correlation matrix of a totally uncorrelated data set, for which  $S = \ln[N]$ .

### B. Simple possible ways to frame a general data set in terms of “events” for the Guttman scaling description

An important question is certainly how a given data set, given as in Eq. (S1), can be described in terms of events and thus to allow an indicator matrix representation. Below we summarize two possible procedures to do so.

The first is when we can associate phenomenological behavior to the data. Then, we can define an event by classifying *appropriate* (i.e., easier to characterize in terms of ranking of predominance) information which can be inferred once we know the explicit values of the  $x_i^{(j)}$ 's. For example, suppose whenever  $x_i^{(j)}$  is above a threshold  $\gamma$ , we can conclude it has been a high electrical pulse crossing the population  $i$  at the measurement step  $j$ . Then, an event could be the existence (1) or not (0) of an intense pulse. Further, suppose that a determined biochemical reaction takes place when  $\alpha < x_i^{(j)} < \beta$ . Such reaction could also constitute another event, with the values 0 and 1 being ascribed conforming to the numerical intervals for the  $x_i^{(j)}$ 's. Importantly, if  $\langle x_i \rangle < \gamma < \alpha$ , in principle we may expect an order of priority between the high pulse and the biochemical reaction. In this way, we might try to organize the events as in Table I according to the numerical sequences in Eq. (S1). Of course, such an approach is heavily based on the concrete understanding of the physical, chemical, biological, etc., aspects underlying the problem studied. In the absence of this type of knowledge, the protocol is not feasible.

A second possibility is to consider an algorithmically oriented method, not relying on any *a priori* qualitative information about the process. But then, admittedly it has a higher chance of not satisfying the perfect homogeneous Guttman scaling [38, 43]. For the full data set, let us define  $a$  and  $b$  as the minimum and maximum values assumed by the entire collection of  $x_i^{(j)}$ 's. Thus, we divide  $[a, b]$  into  $N + 1$  intervals  $\Delta_0, \Delta_1, \dots, \Delta_N$ .

Table II. Consider that for a data set of  $N = 3$  and  $n = 4$ , the twelve  $x_i^{(j)}$ 's assume  $M_0 = 6$ ,  $M_1 = 3$ ,  $M_2 = 2$ ,  $M_3 = 1$  values, respectively, in the numerical intervals  $\Delta_0$ ,  $\Delta_1$ ,  $\Delta_2$  and  $\Delta_3$ . Then, taking as the events the instances (irrespective of  $i$  and  $j$ ) in which the variables are within  $\Delta_1$ ,  $\Delta_2$  and  $\Delta_3$ , one can construct an indicator matrix exactly satisfying a homogeneous Guttman scaling. Indeed, the three, two and one “1”'s in the columns Event 1, Event 2 and Event 3, correspond to  $M_1$ ,  $M_2$  and  $M_3$ , whereas the total of six “0”'s spread in the whole table are due to  $M_0$ .

Pattern	Event 1: Interval $\Delta_1$	Event 2: Interval $\Delta_2$	Event 3: Interval $\Delta_3$	Occurrence of the pattern
1	0	0	0	1
2	1	0	0	1
3	1	1	0	1
4	1	1	1	1

Here,  $\Delta_0$  must represent the most frequent numerical interval for the data set, with the other  $\Delta_i$ 's presenting a decreasing order of occurrence with  $i$ . The events to be considered in the indicator matrix are the occurrence of the intervals  $\Delta_1, \Delta_2, \dots, \Delta_N$  ( $\Delta_0$  is not explicitly included in the events table, but it contributes with the “0”'s in it). For  $M_i$  the number of times the interval  $\Delta_i$  appears in the data set, we have  $\sum_{i=0}^N M_i = n \times N$ . All the incidences  $M_i$ 's ( $i = 0, 1, \dots, N$ ) of the events  $\Delta_i$ 's should thus be combined to generate a structure like that in Table I. An illustration of how to proceed in the particular case the data allows an exact homogeneous Guttman scaling is depicted in Table II. Finally, given that there is a certain freedom in choosing the intervals  $\Delta_i$ 's, this must be done in such way to get an indicator matrix as close as possible to the pattern in Table I.

## II. DATA ACQUISITION

A total of 9 healthy adults (5 women) with no history of neurological or psychiatric disorders (assessed by DSM-IV structured interview [50]), volunteered to ingest 120–200 mL (2.2 mL/kg of body weight) of ayahuasca known to contain 0.8 mg/mL of its main psychoactive compound  $N,N$ -dimethyltryptamine (DMT) and 0.21 mg/mL of harmine, a  $\beta$ -carboline which allows for the entrance of DMT into the bloodstream [51]. The volunteers were assigned with two task-free fMRI sessions: the first one prior to the ayahuasca ingestion, and the second one at 40 minutes after the brew intake (when the acute effects of ayahuasca start to emerge, lasting for approximately 4 hours). Both sessions required the participants to maintain an awake resting state. The experimental procedure was approved by the

Ethics and Research Committee of the University of São Paulo at Ribeirão Preto (No. 14672/2006).

The fMRI images were acquired in a 1.5 T scanner (Siemens, Magnetom Vision), using an EPI-BOLD sequence to obtain 150 volumes with parameters TR = 1700 ms, TE = 66 ms, FOV = 220 mm, matrix  $64 \times 64$ , and voxel dimensions of  $1.72 \text{ mm} \times 1.72 \text{ mm} \times 1.72 \text{ mm}$ . The images were preprocessed in the FSL software [52], and consisted of slice-timing, head motion, and spatial smoothing corrections (Gaussian kernel, FWHM = 5 mm). A total of 9 regressors were used within a general linear model (GLM): 6 regressors to movement correction; 1 to white matter signal; 1 to cerebrospinal fluid; and 1 to global signal. The images were normalized to the standard anatomical space of the Montreal Neurological Institute (MNI152 template) [53].

The preprocessed fMRI images were then parcellated into 110 anatomical regions of interest (ROIs) in accordance with the Harvard-Oxford cortical and subcortical atlas (see Table III). Due to acquisition limitations, six regions were excluded from further analysis. Thus, for each one of the remaining 104 ROIs, we averaged the BOLD signal of the regions's associated voxels, resulting in time courses listing a sequence of  $n = 150$  data points. To reduce confounders in the signal, a maximum overlap discrete wavelet transform (MODWT) was applied to the series in order to select the typical frequency range (0.01–0.1 Hz) of the resting state signal [54]. Finally, in possession of the  $N = 104$  time series  $\mathbf{x}_i$ , we pairwise-correlated them using the Pearson correlation coefficient of Eq. (3) from the main text, resulting in the  $104 \times 104$  Pearson correlation matrix  $\mathbf{R}$ . We thus ended up with a total of 18 functional connectivity networks: two conditions (before and after ayahuasca) for each of the 9 subjects involved.



Table III. Brain regions in accordance with the Harvard-Oxford cortical atlas. Asterisks (\*) are assigned to the six excluded regions. Ordered pairs  $(\ell, r)$  refers to the left ( $\ell$ ) and right ( $r$ ) hemispheres of the corresponding region. For example, in reference to Eq. (3) of the main text, the correlation between the left Thalamus ( $\ell = 97$ ) and right Hippocampus ( $r = 108$ ) is given by the Pearson coefficient  $R_{97,108}$ .

Index	Region
(1, 2)	Frontal Pole
(3, 4)	Insular Cortex
(5, 6)	Superior Frontal Gyrus
(7, 8)	Middle Frontal Gyrus
(9, 10)	Inferior Frontal Gyrus, pars triangularis
(11, 12)	Inferior Frontal Gyrus, pars opercularis
(13, 14)	Precentral Gyrus
(15, 16)	Temporal Pole
(17, 18)	Superior Temporal Gyrus, anterior division
(19, 20)	Superior Temporal Gyrus, posterior division
(21, 22)	Middle Temporal Gyrus, anterior division
(23, 24)	Middle Temporal Gyrus, posterior division
(25, 26)	Middle Temporal Gyrus, temporooccipital part
(27, 28)	Inferior Temporal Gyrus, anterior division*
(29, 30)	Inferior Temporal Gyrus, posterior division
(31, 32)	Inferior Temporal Gyrus, temporooccipital part
(33, 34)	Postcentral Gyrus
(35, 36)	Superior Parietal Lobule*
(37, 38)	Supramarginal Gyrus, anterior division
(39, 40)	Supramarginal Gyrus, posterior division
(41, 42)	Angular Gyrus
(43, 44)	Lateral Occipital Cortex, superior division
(45, 46)	Lateral Occipital Cortex, inferior division
(47, 48)	Intracalcarine Cortex
(49, 50)	Frontal Medial Cortex
(51, 52)	Juxtapositional lobule cortex (form. supp. motor cortex)
(53, 54)	Subcallosal Cortex
(55, 56)	Paracingulate Gyrus
(57, 58)	Cingulate Gyrus, anterior division
(59, 60)	Cingulate Gyrus, posterior division
(61, 62)	Precuneous Cortex
(63, 64)	Cuneal Cortex
(65, 66)	Frontal Orbital Cortex
(67, 68)	Parahippocampal Gyrus, anterior division
(69, 70)	Parahippocampal Gyrus, posterior division
(71, 72)	Lingual Gyrus
(73, 74)	Temporal Fusiform Cortex, anterior division*
(75, 76)	Temporal Fusiform Cortex, posterior division
(77, 78)	Temporal Occipital Fusiform Cortex
(79, 80)	Occipital Fusiform Gyrus
(81, 82)	Frontal Operculum Cortex
(83, 84)	Central Opercular Cortex
(85, 86)	Parietal Operculum Cortex
(87, 88)	Planum Polare
(89, 90)	Heschl's Gyrus (includes H1 and H2)
(91, 92)	Planum Temporale
(93, 94)	Supracalcarine Cortex
(95, 96)	Occipital Pole
(97, 104)	Thalamus
(98, 105)	Caudate
(99, 106)	Putamen
(100, 107)	Pallidum
(101, 108)	Hippocampus
(102, 109)	Amygdala
(103, 110)	Accumbens